Crystal Structure of Human Insulin-like Growth Factor-1: Detergent Binding Inhibits Binding Protein Interactions‡

Felix F. Vajdos,§ Mark Ultsch,§ Michelle L. Schaffer,§ Kurt D. Deshayes,§ Jun Liu,|| Nicholas J. Skelton,§ and Abraham M. de Vos*,§

Departments of Protein Engineering and of Pharmaceutical Research and Development, Genentech, Inc., 1 DNA Way, South San Francisco, California 94080

Received May 3, 2001; Revised Manuscript Received July 14, 2001

ABSTRACT: Despite efforts spanning considerably more than a decade, a high-resolution view of the family of proteins known as insulin-like growth factors (IGFs) has remained elusive. IGF-1 consists of three helical segments which are connected by a 12-residue linker known as the C-region. NMR studies of members of this family reveal a dynamic structure with a topology resembling insulin but little structural definition in the C-region. We have crystallized IGF-1 in the presence of the detergent deoxy big CHAPS, and determined its structure at 1.8 Å resolution by multiwavelength anomalous diffraction, exploiting the anomalous scattering of a single bromide ion and six of the seven sulfur atoms of IGF-1. The structure reveals a well-defined conformation for much of the C-region, which extends away from the core of IGF-1 and has residues known to be involved in receptor binding prominently displayed in a type II β-turn. In the crystal, these residues form a dimer interface, but analytical ultracentrifugation experiments demonstrate that at physiological concentrations IGF-1 is monomeric. A single detergent molecule contacts residues known to be important for IGF-1 binding protein (IGFBP) interactions. Biophysical and biochemical data show that the detergent binds to IGF-1 specifically and blocks binding of IGFBP-1 and IGFBP-3.

Insulin-like growth factor-1 (IGF-1)[1] and insulin-like growth factor-2 (IGF-2) are two closely related proteins (72% identical) which together are strongly structurally and functionally homologous with insulin. Despite the high degree of sequence similarity between IGFs and insulin (∼50%), distinct functional differences exist between the IGFs and insulin. Whereas insulin is primarily a metabolic hormone which regulates glucose homeostasis, IGF-1 is a pleiotropic cytokine that is involved in a wide variety of both developmental and metabolic processes. In contrast to insulin, which acts systemically, IGFs act in both systemic and paracrine/autocrine signaling pathways (reviewed in refs *1* and *2*). In the developing embryo, the absence of IGF-1 leads to severe growth retardation which continues postnatally (*3*−*6*). While most (>75%) of the serum IGF-1 is produced by the liver in response to growth hormone, this liver-derived IGF-1 has been shown to be unnecessary for postnatal body growth in mice (*7*). Rather, it is the locally produced, nonhepatic IGF-1, acting in a paracrine/autocrine manner, which appears to be responsible for most of the postnatal growth-promoting effects of IGF-1 (*8*, *9*). Consistent with its growth-promoting effects, IGF-1 is a powerful mitogen, regulating diverse cellular functions such as cell cycle progression, apoptosis, and cellular differentiation (reviewed in refs *10* and *11*).

The biological effects of IGF-1 are mediated through signaling mechanisms originating from the IGF-1 receptor (IGFR) (reviewed in ref *10*). The IGFR, a receptor tyrosine kinase similar to the insulin receptor (IR), is composed of two disulfide-linked $\alpha-\beta$ heterodimers. The α-chains are predominantly extracellular, and comprise most of the ligand-binding surface. The β-chains are only partially extracellular, and contain the transmembrane segment as well as the cytoplasmic tyrosine kinase domain. As in the insulin−IR complex, IGF-1 binds to the IGFR with a 1:2 stoichiometry (reviewed in ref *12*), with a high-affinity site ($K_d \sim 0.4$ nM) and a low-affinity site ($K_d \sim 6$ nM) (*13*). While IGF-1 is able to bind to the IR with low affinity (*14*−*16*), the role of this interaction is poorly understood, and it is generally accepted that the biological effects of IGF-1 are mediated through the IGFR.

Serum concentrations of free IGF-1 are normally very low due to the presence of a family of binding proteins known as IGFBPs, which bind to IGF-1 with dissociation constants in the low nanomolar range (*17*−*20*). To date, six IGFBPs have been identified, and the binding of IGF-1 to two of these, IGFBP-1 and IGFBP-3, has been extensively characterized (*18*). While the exact biological function of the

‡ The coordinates of IGF-1 have been deposited in the Protein Data Bank as entry 1imx.

* To whom correspondence should be addressed. Telephone: (650) 225-2523. Fax: (650) 225-3734. E-mail: devos@gene.com.

§ Department of Protein Engineering.

|| Department of Pharmaceutical Research and Development.

[1] Abbreviations: IGF, insulin-like growth factor; NMR, nuclear magnetic resonance; deoxy big CHAPS, *N*,*N*-bis(3-D-gluconamidopropyl)deoxycholamide; IGFBP, insulin-like growth factor binding protein; IGFR, insulin-like growth factor receptor; IR, insulin receptor; NOE, nuclear Overhauser effect; MAD, multiwavelength anomalous diffraction; PEG, polyethylene glycol; MPD, methylpentanediol; PBS, phosphate-buffered saline; ELISA, enzyme-linked immunosorbent assay.

10.1021/bi0109111 CCC: $20.00
Published on Web 08/18/2001

IGFBPs is not well understood, it seems clear that at least one role is to sequester IGF-1 in an inactive ternary complex of IGF-1, IGFBP, and a third protein, the acid labile subunit (reviewed in ref *10*). Under certain metabolic conditions, IGFBP-specific proteases release free IGF-1 from the ternary complex by cleaving the bound IGFBP (*10*). In addition, there is evidence that IGFBPs may potentiate IGF-1 activity, enhancing delivery of IGF-1 to the cell surface for interaction with the IGF-1 receptor (*10*). Because of this large pool of IGF-1 in serum, and because of the role of IGF-1 in mediating both insulin-like and mitogenic effects in vivo, the IGFBPs have emerged as targets of indirect agonist drug design (*21*).

Until recently, no crystal structures of either IGF-1 or IGF-2 existed. Consequently, all structural information regarding this family of proteins comes either from early attempts at homology modeling using the known structure of insulin (*22*) or from NMR studies (*23*−*27*). However, IGF-1 is highly dynamic in solution and also prone to aggregation, resulting in very broad line widths at neutral pH (*23*). Hence, all NMR work has been performed at low pH, where IGF-1 is monomeric (*23*−*26*, *28*). Still, these experiments have been plagued by the relatively small number of NOEs (*23*), and the resulting structures are poorly defined. The IGFs and insulin each consist of a small hydrophobic core formed by three helices stabilized by three disulfide bonds; in the single-chain IGFs, these disulfide bonds are intramolecular, while in insulin, they connect the A and B chains. The loop connecting the A and B regions in the IGFs (IGF-1 residues 29−41) is known as the C-region. This loop is analogous to the C-peptide of proinsulin, which is excised during formation of the native hormone. Intriguingly, the C-region of IGF-1 appears to be largely responsible for IGFR specificity (*14*−*16*), with mutation of Tyr 31 reducing the affinity of IGF-1 for the IGFR, while having very little effect on IR binding (*15*). In contrast to the effect on IGFR binding, mutations or deletions in the C-region of IGF-1 have no significant effect on IGFBP interactions (*14*−*16*, *21*). In addition to the C-region, IGF-1 and IGF-2 differ from insulin at their C-termini by a short extension of eight and six residues, respectively, which has been named the "D-region". Mutations or deletions in the D-region have no effect on IGFR binding, but rather enhance affinity for the IGFBPs (*14*). Little is known about the structures of the C- and D-regions, however, as they are essentially undefined by the NMR data (*23*−*27*).

To better understand its unique biological features, especially its interactions with both IGFBPs and the IGFR, we have crystallized IGF-1 and have determined the structure using multiwavelength anomalous diffraction (MAD) at 1.8 Å resolution by exploiting the anomalous scattering of a single bromide ion and six of the seven sulfur atoms of IGF-1. The C-region of IGF-1, which is ordered in the crystal structure, forms a type II β-turn and mediates a crystal packing interaction across a crystallographic dyad. We have characterized the solution state of IGF-1 by analytical ultracentrifugation, and our results indicate that IGF-1 exists primarily as a monomer at neutral pH, with only a slight tendency to dimerize at millimolar concentrations. A detergent molecule, deoxy big CHAPS, mediates a crystal packing contact between symmetry-related molecules and interacts with residues implicated in IGFBP binding. Solution experiments confirm that the IGF-1−deoxy big CHAPS complex does form in solution, and that detergent binding measurably blocks IGFBP binding.

MATERIALS AND METHODS

Crystallization and Data Collection. Recombinant IGF-1 was obtained from Genentech Process Sciences. The initial isolation of IGF-1 from *Escherichia coli* was achieved using aqueous two-phase separation (*29*), followed by refolding (*30*), and subsequent chromatographic purification, including large-scale reverse-phase high-performance liquid chromatography (*31*). Prior to crystallization, IGF-1 was desalted into 0.15 M NaCl and 20 mM sodium acetate (pH 4.5) and diluted to a final concentration of 10 mg/mL. Initially, crystallization trials were set up in the presence of 1 mM IGF-1-binding peptide. However, no peptide was ever observed in the crystal, and crystals grown in the absence of peptide were later shown to be isomorphous to the specimen reported here. A 4 μL droplet of IGF-1 was mixed with 5 μL of reservoir solution [24% PEG 3350 and 0.1 M sodium cacodylate (pH 6.5)] and 1 μL of 14 mM deoxy big CHAPS detergent (Hampton Research, Inc., Laguna Nigel, CA). This solution was allowed to equilibrate by vapor diffusion with 1 mL of reservoir solution. Small, thin plates formed within 4−5 days. At this point, 2 μL of 100% MPD was added, and the crystals dissolved overnight. Within 1 week, crystals reappeared and grew to final dimensions of 0.2 mm × 0.1 mm × 0.05 mm with noticeably sharper edges. These crystals were used for all subsequent analysis.

A single crystal was transferred from the mother liquor to a cryoprotectant solution consisting of 25% (w/v) PEG 3350, 30% MPD, 0.2 M sodium cacodylate (pH 6.5), 2.8 mM deoxy big CHAPS, and 1 M NaBr. After 30 s in this solution, the crystal was flash-cooled by plunging it into liquid nitrogen. All data were collected at 100 K. A four-wavelength MAD data set was collected at beamline 9-2 at the Stanford Synchrotron Radiation Laboratory, with the order of the data sets as follows: Br peak (λ1), low-energy remote (λ2), Br inflection (λ3), and high-energy remote (λ4). The Br peak and inflection points were estimated from fluorescence scans of the crystal, and the low-energy remote was chosen to be 1.54 Å, to optimize the small sulfur anomalous signal at this wavelength while minimizing absorption effects. No inverse beam geometry was used. Data reduction was performed using Denzo and Scalepack (*32*). To determine the most accurate scale and *B*-factors possible, data for all four wavelengths were initially scaled together, assuming no anomalous signal. The scale and *B*-factors determined from this scaling run were then applied to each of the four data sets. Data statistics are reported in Table 1. The crystals belong to space group $C222_1$, with the following unit cell dimensions: $a = 31.83$ Å, $b = 71.06$ Å, and $c = 66.00$ Å. The crystals contain one IGF-1 molecule in the asymmetric unit. The solvent content of the crystals is ~55%.

Structure Determination. Initial attempts to determine the structure of IGF-1 by molecular replacement, using either the available NMR models of IGF-1 or the crystal structure of insulin, were unsuccessful. For this reason, the structure was determined de novo by Br MAD (*33*). The coordinates of the single bound bromide were determined by manual inspection of the anomalous and dispersive difference

Table 1: Crystallographic Statistics for IGF-1

(A) Data Statistics

	λ1	λ2	λ3	λ4
wavelength (Å)	0.9197	1.5406	0.9199	0.8610
resolution (Å)	20−1.80 (1.83−1.80)[a]	20−2.0 (2.03−2.00)	20−1.8 (1.83−1.80)	20−2.0 (2.03−2.00)
no. of observations	44364	30799	44573	32640
no. of unique reflections[b]	6958	5025	6982	5163
R_{merge}[c]	0.044 (0.455)	0.040 (0.117)	0.038 (0.290)	0.038 (0.135)
completeness (%)	98.3 (97.9)	96.1 (93.1)	98.2 (99.1)	98.8 (99.4)
$I/\sigma(I)$	8.1	10.9	9.1	10.2

(B) MAD Phasing

	λ1			λ2			λ3			λ4		
	A[d]	C[d]	Ano[d]	A	C	Ano	A	C	Ano	A	C	Ano
R_{Cullis}[e]	−	−	0.84	0.52	0.56	0.94	0.62	0.68	0.92	0.61	0.66	0.91
phasing power[f]	−	−	1.41	2.80	1.83	1.12	2.32	1.50	1.07	1.85	1.19	1.24
no. of sites	1 Br, 6 S											
occupancies[g]	0.70 (Br), 1.0 (S)											
overall FOM	0.58 (A), 0.50 (C)											

(C) Refinement Statistics

R_{cryst}[h]	0.247
R_{free}[h]	0.259
no. of protein atoms	432
no. of detergent atoms	60
no. of waters	47
no. of Br atoms	1
$\langle B_{protein} \rangle$ (Å^2)	30.4
$\langle B_{detergent} \rangle$ (Å^2)	43.3
$\langle B_{water} \rangle$ (Å^2)	41.3
rmsd for bond lengths (Å)	0.006
rmsd for angles (deg)	1.054
rmsd for bonded B's (Å^2)	1.65

[a] High-resolution shell. [b] Unique reflections assuming Friedel symmetry. [c] $R_{merge} = \sum_{hkl}(|I_{hkl} - \langle I_{hkl} \rangle|)/\sum_{hkl}\langle I_{hkl} \rangle$, where I_{hkl} is the intensity of reflection *hkl* and $\langle I_{hkl} \rangle$ is the average intensity of multiple observations. [d] A, acentric reflections; C, centric reflections; Ano, anomalous differences. [e] $R_{Cullis} = \sum||F_{ph} - F_p| - |F_{h(calc)}||/|F_{ph} - F_p|$, where F_{ph}, F_p, and F_h are the "derivative", "native", and calculated heavy-atom structure factors, respectively. Native in this case refers to the reference data, derivative to the other data sets, and F_h to the dispersive or Bijvoet differences. [f] Phasing power $= \sum|F_h|/\sum|F_{ph(obs)} - F_{ph(calcd)}|$, where F_{ph} and F_h are the derivative and calculated heavy-atom structure factors, respectively. [g] Occupancies of the atoms used for phase refinement. Refined after data were placed an approximately absolute scale. [h] $R_{cryst} = \sum|F_o - F_c|/\sum F_o$, where F_o and F_c are the observed and calculated structure factor amplitudes, respectively. R_{free} is the *R*-factor for a randomly selected 8% of reflections which were not used in the refinement.

Patterson maps. The hand ambiguity was resolved by phase refinement using SHARP (*34*), followed by examination of anomalous difference Fourier maps calculated using the λ2 Bijvoet differences. A cluster of six peaks for one hand of the Br coordinates was consistent with the disulfide structure of insulin (PDB entry 1ZNI). These six peaks correspond to the six Cys Sγ atoms in IGF-1; a seventh sulfur (Met 59 Sδ) was never detected in anomalous difference Fourier maps, presumably due to its higher temperature factor (36.7 Å^2). At this point, the six Cys Sγ positions were included in the phase refinement, with the λ1 data set used as a reference. Throughout the phase refinement, the Br f'' was refined for the λ1 data set, f' and f'' were refined for λ3, and both were kept fixed for data sets λ2 and λ4; the f'' and f' values for sulfur were kept fixed at the theoretical values for each wavelength. The small anomalous signal from the sulfur atoms had a modest effect on the phasing statistics, but the resulting electron density maps exhibited improved connectivity, especially in the less well-ordered regions of IGF-1. Density modification (solvent flattening and histogram mapping) was performed using DM (*35*, *36*), and the resulting electron density maps were of high quality. Approximately 50% of the structure, corresponding to the three helical regions of IGF-1, was built directly into the experimental electron density maps using the programs O (*37*) and QUANTA (version 97.0, MSI, San Diego, CA). Several rounds of phase combination using Sigmaa (*36*, *38*) allowed the remainder of the molecule to be modeled. Atomic positional and restrained *B*-factor refinement utilized the maximum likelihood target function of CNX (ref *39* and MSI), coupled with a "mask"-type bulk solvent correction and anisotropic overall *B*-factor scaling. The final model contains residues 3−34 and 41−64 of IGF-1, one deoxy big CHAPS molecule, one Br$^-$, and 50 water molecules. Refinement statistics are reported in Table 1C. The model was refined against the λ3 data set, since the data statistics demonstrated that this data set is of higher quality than the others (Table 1A). All data from 20 to 1.8 Å resolution were included in the refinement, and no σ cutoff was applied. Secondary structure assignments were made with PROMOTIF (*37*, *40*). Figures 1 and 2 were prepared using MOLSCRIPT (*41*) and RASTER3D (*42*); Figure 3 was prepared using INSIGHT (MSI).

IGF-1 Phage ELISA. E. coli cells (XL1-Blue, Stratagene), freshly transformed with the phage vector pIGF-g3 displaying human IGF-1 as described in ref *18*, were grown overnight in 5 mL of 2YT medium (*43*). The phage particles displaying IGF-1 were titered against IGFBP-1 and IGFBP-3 for a 500−1000-fold dilution for preincubation with serial dilutions of deoxy big CHAPS and binding protein standards for 45 min.

Maxisorp immunoplates (Nunc) were coated with IGFBP-1 or IGFBP-3 overnight at 4 °C [50 μL at a concentration of 3 μg/mL in 50 mM carbonate buffer (pH 9.6)], blocked with 0.5% Tween 20 and PBS, and washed eight times with PBS and 0.05% Tween 20. The samples were added to the plates for 30 min. Plates were washed eight times with PBS and 0.05% Tween 20, incubated with 50 μL of a 1:10000 horseradish peroxidase−anti-M13 antibody conjugate (Amersham Pharmacia Biotech, Piscataway, NJ) in PBS and 0.5% BSA for 30 min, and then washed eight times with PBS and 0.05% Tween 20 and two times with PBS. Plates were developed using a tetramethylbenzidine substrate (Kirkegaard and Perry, Gaithersburg, MD); the reactions were stopped with 1.0 M H_3PO_4, and the plates were read spectrophotometrically at 450 nm.

Diffusion-Based Assessment of Detergent Binding. NMR-derived diffusion measurements were used to estimate the K_d for the interaction between IGF-1 and deoxy big CHAPS. Samples were prepared in 50 mM phosphate buffer in D_2O (pH 6.5, uncorrected meter reading) and contained 1.0 mM deoxy big CHAPS with 0.5 mM IGF-1, 0.5 mM deoxy big CHAPS with 0.25 mM IGF-1, 0.25 mM deoxy big CHAPS with 0.125 mM IGF-1, or deoxy big CHAPS only (1.0, 0.5, or 0.25 mM). All spectra were acquired at 40 °C on a Bruker Avance 500 spectrometer equipped with a 5 mm triple-axis gradient, triple-resonance probe. Diffusion measurements were taken with a bipolar pulse pair method where $\delta = 5$ ms, $\tau = 2$ ms, and $\Delta = 25$ or 40 ms for deoxy big CHAPS alone or deoxy big CHAPS with IGF-1, respectively (*44*). Spectra were collected with 128−1024 transients as the *z*-gradient strength was increased from 0.009 to 0.45 T m^{-1} in 18 equal increments; measurements were taken at least twice on each sample. Spectra were processed and peak heights extracted with the program FELIX (version 98.0, MSI). Diffusion constants, the proportion of bound detergent, and the resulting K_d were extracted as described by Fejzo et al. (*45*). Two-dimensional NOESY spectra (*46*) were collected on a 0.5 mM sample of IGF-1 in the presence or absence of 1.0 mM deoxy big CHAPS detergent with a mixing time of 100 ms.

Sedimentation Equilibrium Analysis. The self-association of IGF-1 was assessed by sedimentation equilibrium analysis. The experiments were conducted at 20 °C in a Beckman XLA/I analytical ultracentrifuge. The samples were prepared in 0.1 M citrate buffer (pH 6.5) and 75 mM NaCl with a loading concentration from 1 to 0.01 mM. The concentration gradients were measured at rotor speeds of 25 000 and 30 000 rpm at 280 or 285 nm using a scanning absorption optical system. The attainment of an equilibrium state was verified by comparing successive scans after approximately 16 h. The partial specific volume of IGF-1 was calculated from its amino acid composition. The data were fit as a single ideal species or the ideal dimer self-association models using a nonlinear least-squares fitting program, NONLIN (*47*). The association constants were determined from the best-fit values of the model, returned by nonlinear least-squares regression.

RESULTS

Description of the Structure. IGF-1 is composed primarily of three helical segments corresponding to the B-helix (IGF-1 residues 7−18) and two A-helices (IGF-1 residues 43−47 and 54−58) of insulin (Figure 1). The hydrophobic core is essentially identical to that described for the NMR structures of IGF-1, including the three disulfide linkages between Cys 6 and Cys 48, Cys 18 and Cys 61, and Cys 47 and Cys 52 (*23*−*26*). Residues 3−6 do not form any regular secondary structure, and hence, the structure described here can be classified as being most similar to the T-form of insulin (*48*). Indeed, when IGF-1 and the T-form of insulin are superimposed on the Cα positions of their respective helical segments (IGF-1 residues 8−19, 42−49, and 54−61 and insulin residues B9−B20, A1−A8, and A13−A20), the rmsd is only 0.47 Å. As in insulin, residues 18−21 at the end of the B-helix form a type II′ β-turn, which redirects the backbone from the B-helix into an extended region. Residues 24−27 form a type VIII β-turn to accommodate the C-region, which extends away from the core of IGF-1, and interacts with a symmetry-related molecule (see below). Residues 30−33 form a well-defined type II β-turn, prominently displaying Tyr 31 at the $i + 1$ position (Figure 1). Residues 35−40 have not been modeled, as the electron density in this region is weak and disconnected. Of the D-region, only the first two residues, 63 and 64, are ordered in the structure.

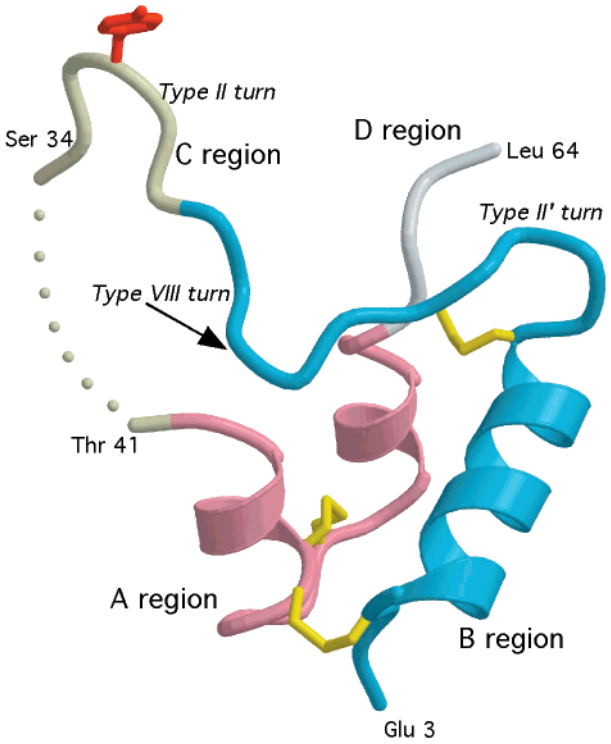

FIGURE 1: Ribbon structure of IGF-1. The B-region (residues 3−28) is shown in blue, the C-region (residues 29−41) in light yellow, the A-region (residues 42−62) in pink, and the D-region (residues 63 and 64) in white. The three β-turns described in the text are labeled in italics. The three disulfides (Cys 6−Cys 48, Cys 18−Cys 61, and Cys 47−Cys 52) are shown as yellow sticks. Tyr 31 is shown in red at the tip of the C-region.

The C-region of IGF-1 mediates a 2-fold symmetric crystal packing interaction across the *a*-axis of the unit cell (Figure 2). This interaction buries 689 Å^2 of solvent-accessible surface area from each molecule of IGF-1, or 1378 Å^2 total, and is the largest interface in the crystal. A total of 28 intermolecular contacts ≤3.6 Å in length are formed via this interface, with the next most extensive crystal packing interaction forming only nine contacts. The core of the

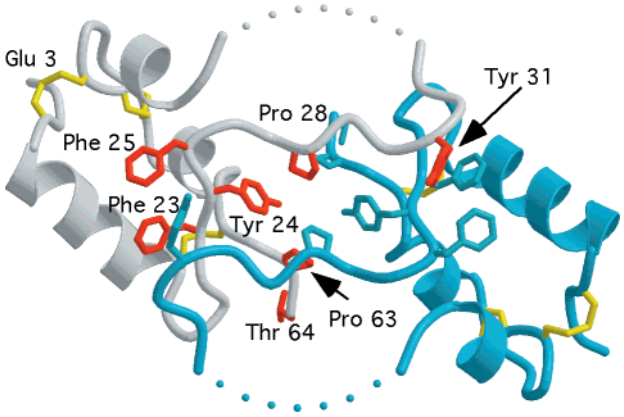

FIGURE 2: Crystallographic dimer of IGF-1. One monomer is depicted in gray, the other in blue. The residues which are partially buried by the dimer interface are labeled for one of the monomers and are depicted in red. For reference, the N-terminal Glu 3 is indicated for one monomer. The dashed lines indicate the disordered region from residue 35 to 40 in each monomer.

interface is dominated by Tyr 24 and Pro 28 from each monomer, which bury 39 and 57 Å^2 of solvent-accessible surface area, respectively. The aromatic ring of Tyr 31, which lies at the tip of the loop at the furthest point from the core of IGF-1, packs against the phenolic rings of Phe 23 and Phe 25 of the symmetry-related molecule. In addition to these hydrophobic interactions, two main chain hydrogen bonds (Tyr 31 N···Phe 23 O and Ser 34 N···Asp 20 O) are present in the dimer interface. Residues from the D-region (62−64) are also partially sequestered by this dimer formation. Because of these interactions, most of the C-region in the crystal is well-ordered, providing the first high-resolution view of the conformation of this biologically important loop.

A single molecule of deoxy big CHAPS interacts with residues forming a small hydrophobic cleft on one surface of IGF-1 (Leu 5, Phe 16, Val 17, Leu 54, and Leu 57) (Figure 3a). The opposite face of the detergent mediates a symmetry contact with residues Val 11, Leu 14, and Gln 15 of a symmetry-related IGF-1 molecule. Intriguingly, this face of deoxy big CHAPS also contacts the edge of the dimer interface, with close contacts to Phe 23 and Phe 25 of the same IGF-1 molecule, as well as Tyr 31 and Gly 32 of the dimeric partner (Figure 3B).

Deoxy Big CHAPS Binds to IGF-1 in Solution. The affinity of IGF-1 for deoxy big CHAPS was ascertained using solution NMR methods. The chemical shift changes observed during a titration of deoxy big CHAPS into a 0.5 mM IGF-1 solution suggested that the affinity was submillimolar (data not shown) and not easily measurable from such data. Instead, diffusion measurements were taken on samples at varying IGF-1 concentrations containing 2 molar equiv of detergent, as well as on several samples of detergent alone (the detergent concentration was always lower than the critical micelle concentration of 1.4 mM for deoxy big CHAPS and CHAPS). The decrease in the diffusion constant of the detergent in the presence of the protein can be used to estimate the proportion of detergent bound to the protein (*45*); since the total concentration of detergent and protein is known, a value of the dissociation constant can be determined. At the three protein concentrations that were studied (0.5, 0.25, and 0.125 mM), K_d values of 220, 440, and 430 μM, respectively, were obtained. This technique has

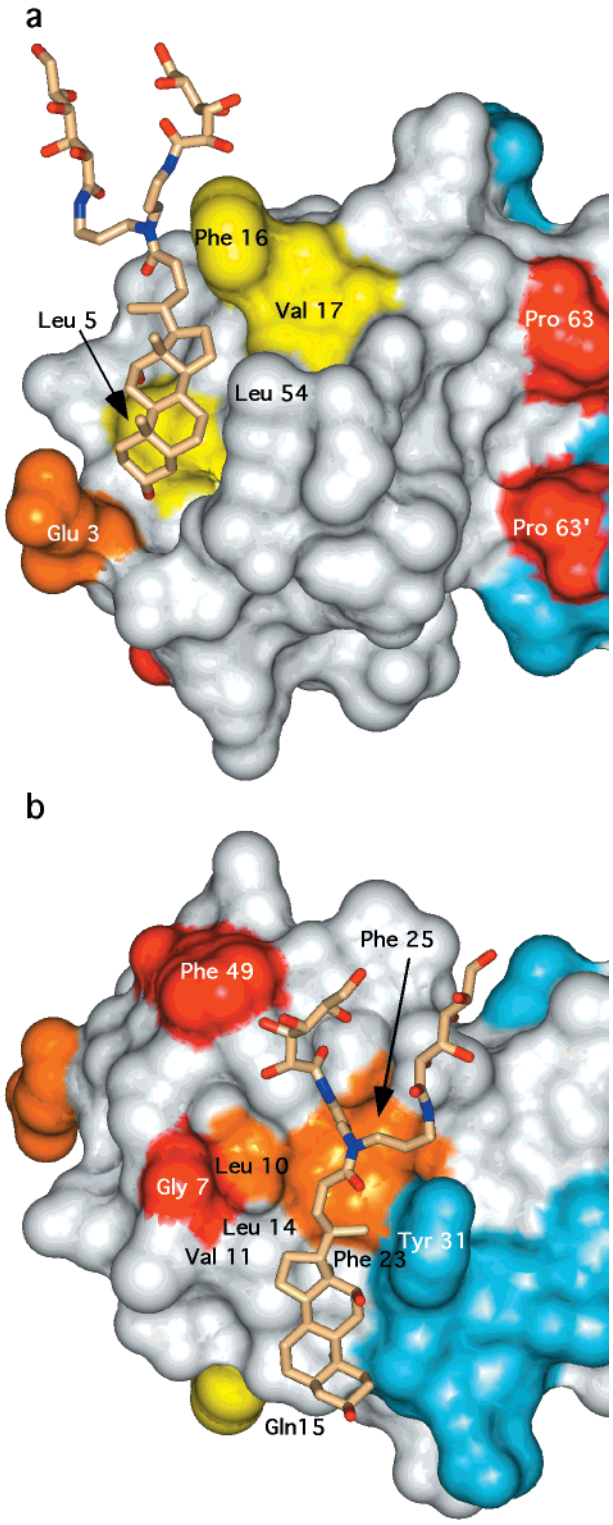

FIGURE 3: Molecule of deoxy big CHAPS binding at a hydrophobic cleft on IGF-1. (a) The molecule of deoxy big CHAPS is depicted in stick form, with the deoxy CHAPS headgroup inserted into the cleft lined by residues Leu 5, Phe 16, Val 17, Leu 54, and Leu 57. The coloring is according to the alanine-scanning mutagenesis results of Dubaquie and Lowman (*18*), with yellow indicating a 5−10-fold reduction, orange a 10−100-fold reduction, and red a >100-fold reduction in affinity for IGFBP-1. The blue surface corresponds to the symmetry-related IGF-1 molecule which forms the crystallographic dimer. (b) View from the opposite face of deoxy big CHAPS showing the interactions of the detergent molecule with a symmetry-related IGF-1 molecule. The color scheme is the same as in panel A.

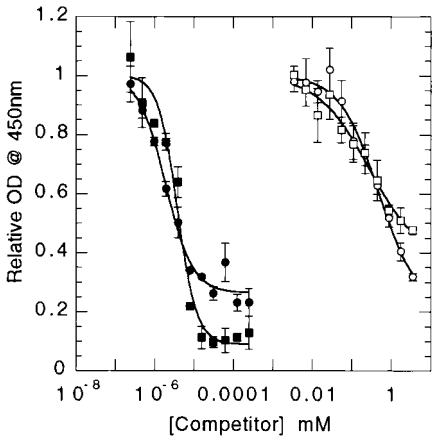

FIGURE 4: Results of the detergent−IGFBP competition binding study. Deoxy big CHAPS detergent was used as a competitive inhibitor of IGF-1 binding to immobilized IGFBP-1 (○) or IGFBP-3 (□). As a positive control, soluble IGFBP-1 (●) or IGFBP-3 (■) was used as a competitive inhibitor of IGF-1 binding to immobilized IGFBP-1 or IGFBP-3, respectively. Each data point represents the average of three independent experiments.

routinely been applied to small molecules (molecular mass of less than or equal to several hundred daltons) binding to large proteins. In this particular case, the ligand is relatively large (862 Da) and the protein is relatively small (7648 Da); hence, the differential decrease in the diffusion constant on binding is small. This increases the uncertainty with which the dissociation constant can be measured. Given this, the data described above suggest that the K_d for the interaction between deoxy big CHAPS and IGF-1 is 300 ± 150 μM.

Deoxy Big CHAPS Blocks IGFBP-1 and IGFBP-3 Binding. To examine the binding epitope of deoxy big CHAPS on IGF-1, we preincubated detergent with IGF-1 expressed on bacteriophage particles and measured the level of residual binding to IGFBP-1 and IGFBP-3 in a plate-based assay (ELISA). As a control, soluble IGFBP-1 was also tested. As shown in Figure 4, deoxy big CHAPS inhibited IGF-1 on phage from binding to IGFBP-1 and IGFBP-3 with IC_{50} values of 480 ± 170 and 275 ± 152 μM, respectively. These numbers must be interpreted conservatively, however, since the critical micelle concentration of deoxy big CHAPS (1.4 mM) presents an upper limit on the curve in Figure 4. Despite the limitations of the experiment, the IC_{50} values obtained for deoxy big CHAPS are in good agreement with our NMR-based estimate of a K_d of ∼300 μM for the deoxy big CHAPS−IGF-1 interaction.

Self-Association of IGF-1. The sedimentation equilibrium data show that IGF-1 undergoes self-association in solution. The average molecular mass increased with increasing protein concentration from 0.01 to 1 mM (data not shown). The average molecular mass at the highest concentration that was studied (1 mM) is ∼37% higher than the monomer molecular mass (10.4 kDa at 1 mM vs 7.6 kDa, the monomer molecular mass). At concentrations of <0.05 mM, no self-association was observed, and IGF-1 exists only as a monomer in solution at neutral pH. If we assume that the higher-molecular mass species are IGF-1 dimers, the sedimentation data can be fit as a monomer−dimer model with a K_d of 3.6 ± 1.0 mM (Figure 5). The presence of 1 mM deoxy big CHAPS did not enhance IGF-1 self-association (data not shown).

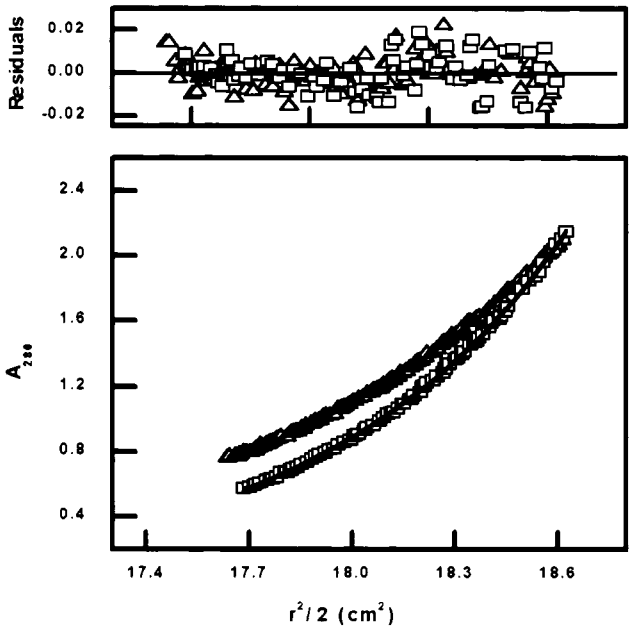

FIGURE 5: Nonlinear least-squares analysis of sedimentation equilibrium data for IGF-1 in solution. Data collected at rotor speeds of 30 000 (△) and 35 000 rpm (□) were fit as an ideal monomer−dimer self-association model. The solid lines are the fits of the data. The residuals are plotted above the figure for both rotor speeds, and are randomly distributed around zero, indicating that the monomer−dimer model is correct for this interaction.

DISCUSSION

C-Region Conformation and the Dimer Interface. The C-region in the IGF-1 crystal structure extends out from the core of the molecule, with residues 30−33 forming a canonical type II β-turn, and the remainder of the C-region forming a crystallographic dimer with a symmetry-related molecule. Tyr 31 has been implicated as being a critical determinant for IGFR binding (*14*−*16*), and its location at the tip of this extension places it in an ideal location to interact with a receptor molecule. While this region of IGF-1 is not well-defined by NMR data, the conformation of the C-region in the crystal is likely to reflect a prevalent solution conformation. There is evidence of a reverse turn at the tip of the loop and a hinge bending at the loop termini of IGF-2 (*27*). Thus, while crystal packing forces undoubtedly help stabilize the orientation of this loop, its conformation appears to be consistent with the solution structure of the closely related IGF-2.

The size of the interface formed by the crystallographic dimer is well within the range of buried surface area in known biological complexes (*49*). In addition, this interaction partially excludes from solvent several of the residues known to be important for binding to the IGFR, including Phe 23 (69% buried), Tyr 24 (64% buried), Phe 25 (29% buried), and Tyr 31 (38% buried). Other groups have also reported homodimeric interactions of IGF-1 and IGF-2. Laajoki et al. report that at a concentration of 1 mM, an engineered form of IGF-1 (Long-[Arg^3]IGF-1) partitions into ∼20% dimer and 80% monomer (*25*), a ratio which is in good agreement with our estimate of a 3.6 mM K_d. In their NMR study of IGF-2, Torres et al. (*27*) reported that the amide protons of residues in the C-region were slowly exchanging with solvent, suggesting that IGF-2 forms a homodimer in

solution. However, despite the significant amount of surface area which is buried upon dimer formation in the crystal, the affinity of IGF-1 for itself is very weak. In addition, the known binding stoichiometry of one IGF-1 molecule per receptor dimer (*12*) makes it difficult to rationalize the biological significance of IGF-1 dimerization. Therefore, we conclude that the IGF-1 dimer in this crystal form results from the high concentration of IGF-1 in the crystallization experiment, and does not represent a physiologically relevant form of the molecule.

Detergent Binding, Crystallization, and NMR Mobility. The very low quality of NMR spectroscopic data obtained for IGF-1 at near-neutral pH has been attributed to a combination of self-association and internal mobility that leads to a large variation in resonance line width (*23*). As a result, NOESY spectra acquired on IGF-1 contain many broad, overlapped peaks and few sharp, well-resolved correlations. NOESY spectra collected for IGF-1 in the presence of an excess of deoxy big CHAPS have a similar appearance. Thus, detergent binding is not sufficient to eliminate the aggregation or inherent flexibility of IGF-1 and does not facilitate characterization of the solution conformation of the protein. Likewise, detergent binding does not alter the aggregation state of IGF-1, as assessed by analytical ultracentrifugation experiments in the presence of deoxy big CHAPS. This is in contrast to observations in the crystalline state where addition of deoxy big CHAPS leads to a well-packed crystallographic dimer and crystals that diffract to high resolution. Why does detergent binding allow IGF-1 to crystallize? Jansson and colleagues noted that the lack of NMR assignments in the region immediately surrounding Cys 6, which includes Leu 5 and Gly 7, was indicative of the Cys 6−Cys 48 disulfide undergoing intermediate exchange between cis and trans configurations (*19*). The fact that the detergent binds to one face of the B-helix immediately opposite this disulfide suggests that it may serve to stabilize this region of the molecule by more complete packing of the hydrophobic cleft. Indeed, in our crystal structure, the Cys 6−Cys 48 disulfide bridge is clearly in the trans configuration, and there is no evidence of multiple conformations.

IGFBP-1 and IGFBP-3 Binding. Several studies have identified residues in IGF-1 which are important for IGFBP binding (*17*−*21*, *50*). Dubaquie and Lowman (*18*) identified two distinct patches on IGF-1 which interact with IGFBP-1 and IGFBP-3. Patch 1 consists of Glu 7, Leu 10, Val 11, Leu 14, Phe 25, Ile 43, and Val 44, while patch 2 consists of Glu 3, Thr 4, Leu 5, Phe 16, Val 17, and Leu 54 (*18*). In the crystal structure of IGF-1, these two patches are involved in detergent-mediated crystal packing contacts. The overlap of the detergent binding site with the IGFBP interaction surfaces is entirely consistent with our observation that deoxy big CHAPS blocks IGFBP-1 and IGFBP-3 binding. In contrast, deoxy big CHAPS does not inhibit IGFR-mediated signaling in a cell-based receptor activation assay (data not shown). These results are consistent with prior studies which demonstrated different binding epitopes on IGF-1 for receptor and IGFBP interactions (*14*−*16*). The identification of deoxy big CHAPS as an inhibitor of IGFBP interactions suggests that it may be possible to develop small molecule drugs which disrupt the IGF-1−IGFBP complex in vivo, thereby releasing receptor-active IGF-1 from the systemic, inactive pool. Such an approach may one day lead to an orally bioavailable therapy for metabolic diseases such as diabetes.

ACKNOWLEDGMENT

We are grateful to J. Stamos, S. G. Hymowitz, and C. W. Eigenbrot for assistance in X-ray data collection, M. Sadick for performing the cell-based IGFR activation assay, R. F. Kelley, P. Lester, and H. B. Lowman for helpful discussions and advice, and the Genentech Department of Process Science for providing the IGF-1 used for all the experiments reported here. This work is based upon research conducted at the Stanford Synchrotron Radiation Laboratory (SSRL), which is funded by the Department of Energy (BES and BER) and the National Institutes of Health (NCRR and NIGMS).

NOTE ADDED IN PROOF

Recently Zeslawski et al. published the crystal structure of IGF-1 in complex with the N-terminal domain of IGFBP-5 (*EMBO J. 20*, 3638−3644). The structure of that complex is entirely consistent with the model of deoxy big CHAPS inhibition of IGFBP binding presented in this manuscript.

REFERENCES

1. Isaksson, O. G. P., Lindahl, A., Nilsson, A., and Isgaard, J. (1987) *Endocr. Rev. 8*, 426−438.
2. Daughaday, W. H., and Rotwein, P. (1989) *Endocr. Rev. 10*, 68−91.
3. Baker, J., Liu, J.-P., Robertson, E. J., and Efstratiadis, A. (1993) *Cell 75*, 73−82.
4. Powell-Braxton, L., Hollingshead, P., Warburton, C., Dowd, M., Pitts-Meek, S., Dalton, D., Gillett, N., and Stewart, T. A. (1993) *Genes Dev. 7*, 2609−2617.
5. Liu, J.-P., Baker, J., Perkins, A. S., Robertson, E. J., and Efstratiadis, A. (1993) *Cell 75*, 59−72.
6. Liu, J.-L., Grinberg, A., Westphal, H., Sauer, B., Accili, D., Karas, M., and LeRoith, D. (1998) *Mol. Endocrinol. 12*, 1452−1462.
7. Sjogren, K., Liu, J.-L., Blad, K., Skrtic, S., Vidal, O., Wallenius, V., LeRoith, D., Tornell, J., Isaksson, O. G. P., Jansson, J.-O., and Ohlsson, C. (1999) *Proc. Natl. Acad. Sci. U.S.A. 96*, 7088−7092.
8. Schlechter, N. L., Russell, S. M., Spencer, E. M., and Nicoll, C. S. (1986) *Proc. Natl. Acad. Sci. U.S.A. 83*, 7932−7934.
9. Isaksson, O. G. P., Jansson, J.-O., and Gause, I. A. M. (1982) *Science 216*, 1237−1239.
10. Jones, J. I., and Clemmons, D. R. (1995) *Endocr. Rev. 16*, 3−34.
11. LeRoith, D. (2000) *Endocrinology 141*, 1287−1288.
12. De Meyts, P. (1994) *Diabetologia 37*, S135−S148.
13. Tollefsen, S. E., and Thompson, K. (1988) *J. Biol. Chem. 263*, 16267−16273.
14. Bayne, M. L., Applebaum, J., Underwood, D., Chicchi, G. G., Green, B. G., Hayes, N. S., and Cascieri, M. A. (1988) *J. Biol. Chem. 264*, 11004−11008.
15. Bayne, M. L., Applebaum, J., Chicchi, G. G., Miller, R. E., and Cascieri, M. A. (1990) *J. Biol. Chem. 265*, 15648−15652.
16. Cascieri, M. A., Chicchi, G. G., Applebaum, J., Hayes, N. S., Green, B. G., and Bayne, M. L. (1988) *Biochemistry 27*, 3229−3233.
17. Clemmons, D. R., Dehoff, M. L., Busby, W. H., Bayne, M. L., and Cascieri, M. A. (1992) *Endocrinology 131*, 890−895.
18. Dubaquié, Y., and Lowman, H. B. (1999) *Biochemistry 38*, 6386−6396.
19. Jansson, M., Andersson, G., Uhlen, M., Nilsson, B., and Kordel, J. (1998) *J. Biol. Chem. 273*, 24701−24707.
20. Oh, Y., Muller, H. L., Lee, D.-Y., Fielder, P. J., and Rosenfeld, R. G. (1993) *Endocrinology 132*, 1337−1344.

21. Lowman, H. B., Chen, Y. M., Skelton, N. J., Mortensen, D. L., Tomlinson, E. E., Sadick, M. D., Robinson, I. C. A. F., and Clark, R. G. (1998) *Biochemistry 37*, 8870−8878.
22. Blundell, T. L., Bedarkar, S., and Humbel, R. E. (1983) *Fed. Proc. 42*, 2592−2597.
23. Cooke, R. M., Harvey, T. S., and Campbell, I. D. (1991) *Biochemistry 30*, 5484−5491.
24. De Wolf, E., Gill, R., Geddes, S., Pitts, J., Wollmer, A., and Grotzinger, J. (1996) *Protein Sci. 5*, 2193−2202.
25. Laajoki, L. G., Francis, G. L., Wallace, J. C., Carver, J. A., and Keniry, M. A. (2000) *J. Biol. Chem. 275*, 10009−10015.
26. Sato, A., Nishimura, S., Ohkubo, T., Kyogoku, Y., Koyama, S., Kobayashi, M., Yasuda, T., and Kobayashi, Y. (1993) *Int. J. Pept. Protein Res. 41*, 433−440.
27. Torres, A. M., Forbes, B. E., Aplin, S. E., Wallace, J. C., Francis, G. L., and Norton, R. S. (1995) *J. Mol. Biol. 248*, 385−401.
28. Laajoki, L. G., Breton, E. L., Shooter, G. K., Wallace, J. C., Francis, G. L., Carver, J. A., and Keniry, M. A. (1997) *FEBS Lett. 420*, 97−102.
29. Hart, R. A., Lester, P. M., Reifsnyder, D. H., Ogez, J. R., and Builder, S. E. (1994) *Bio/Technology 12*, 1113−1117.
30. Hart, R. A., Giltinan, D. M., Lester, P. M., Reifsnyder, D. H., Ogez, J. R., and Builder, S. E. (1994) *Biotechnol. Appl. Biochem. 20*, 217−232.
31. Olson, C. V., Reifsnyder, D. H., Canova-Davis, E., Ling, V. T., and Builder, S. E. (1994) *J. Chromatogr. A675*, 101−112.
32. Otwinowski, Z., and Minor, W. (1997) *Methods Enzymol. 276*, 307−326.
33. Dauter, Z., Dauter, M., and Rajashankar, K. R. (2000) *Acta Crystallogr. D56*, 232−237.
34. De La Fortelle, E., and Bricogne, G. (1997) *Methods Enzymol. 276*, 472−494.
35. Cowtan, K. (1994) *Joint CCP4 and ESF-EACBM Newsletter on Protein Crystallography 31*, 34−38.
36. Collaborative Computational Project Number 4 (1994) *Acta Crystallogr. D50*, 760−763.
37. Jones, T. A., Zou, J. Y., Cowan, S. W., and Kjeldgaard, M. (1991) *Acta Crystallogr. A47*, 110−119.
38. Read, R. J. (1986) *Acta Crystallogr. A42*, 140−149.
39. Brünger, A. T., Adams, P. D., Clore, G. M., DeLano, W. L., Gros, P., Grosse-Kunstleve, R. W., Jiang, J.-S., Kuszewski, J., Nilges, M., Pannu, N. S., Read, R. J., Rice, L. M., Simonson, T., and Warren, G. L. (1998) *Acta Crystallogr. D54*, 905−921.
40. Hutchinson, E. G., and Thornton, J. M. (1996) *Protein Sci. 5*, 212−220.
41. Kraulis, P. J. (1991) *J. Appl. Crystallogr. 24*, 946−950.
42. Merritt, E. A., and Bacon, D. J. (1997) *Methods Enzymol. 277*, 505−524.
43. Sambrook, J., Fritsch, E. F., and Maniatis, T. (1989) *Molecular Cloning: A Laboratory Handbook*, Cold Spring Harbor Laboratory Press, Plainview, NY.
44. Wu, D., Chen, A., and Johnson, C. S. J. (1995) *J. Magn. Reson., Ser. A 115*, 260−264.
45. Fejzo, J., Lepre, C. A., Peng, J. W., Bemis, G. W., Ajay, Murko, M. A., and Moore, J. M. (1999) *Chem. Biol. 6*, 755−769.
46. Jeener, J., Meier, B. H., Bachmann, P., and Ernst, R. R. (1979) *J. Chem. Phys. 71*, 4546−4553.
47. Johnson, M. L., Correia, J. C., Yphantis, D. A., and Halvorson, H. R. (1981) *Biophys. J. 36*, 578−588.
48. Derewenda, U., Derewenda, Z., Dodson, E. J., Dodson, G. G., Reynolds, C. D., Smith, G. D., Sparks, C., and Swenson, D. (1989) *Nature 338*, 594−596.
49. Janin, J., and Chothia, C. (1990) *J. Biol. Chem. 264*, 16027−16030.
50. Dubaquié, Y., Mortensen, D. L., Intintoli, A., Hogue, D. A., Nakamura, G., Rancatore, P., Lester, P., Sadick, M. D., Filvaroff, E., Fielder, P. J., and Lowman, H. B. (2001) *Endocrinology 142*, 165−173.

BI0109111